Heat and freshwater exchange on the Antarctic continental shelf in a regional coupled climate model

Changhyun Yoo[1]*, John M. Klinck[2], Edwin P. Gerber[1], David Holland[1], Michael Dinniman[2], David Bromwich[3,4], Keith Hines[3], and Lesheng Bai[3]

[1]Center for Atmosphere Ocean Science, Courant Institute of Mathematical Sciences, New York University, New York, New York

[2]Department of Ocean, Earth and Atmospheric Sciences Center for Coastal Physical Oceanography, Old Dominion University, Norfolk, Virginia

[3]Polar Meteorology Group, Byrd Polar and Climate Research Center The Ohio State University, Columbus, Ohio

[4]Atmospheric Sciences Program, Department of Geography The Ohio State University, Columbus, Ohio

Submitted to *Journal of Climate*

*Current affiliation: Department of Atmospheric Sciences, Yonsei University, Seoul, South Korea.

Correspondence to: Changhyun Yoo. 549 Science Hall, Department of Atmospheric Sciences, Yonsei University, 50 Yonsei-ro, Seodaemun-gu, Seoul, South Korea 120-749. Email: cyoo@cims.nyu.edu.

Abstract

Understanding heat and freshwater content change in the Antarctic shelf seas is important for the basal melting of ice shelves. This study analyzes the heat and freshwater budget using a regional coupled climate model, which has been optimized for a domain including Antarctica and the bulk of the Southern Ocean. A new technique that utilizes passive tracers is introduced to track the oceanic heat and freshwater transport across the Antarctic continental shelf break.

The surface exchange with the atmosphere and sea ice dominates the annual cycle in heat and freshwater content change in the Antarctic shelf. Oceanic transport, however, provides a near constant source of heat and freshwater to the shelf, balancing a net loss through the surface. Two distinct annual cycles, one above the pycnocline (0-300 m) and the other below (300 m and below) are found. While surface processes dominate the cycle in the upper layer, oceanic transport plays a key role in the variations in the lower layer. Despite lack of interactive ice shelf, the net atmospheric and ocean transports appear sufficiently large to compensate for missing ice shelf thermodynamics and imply that these effects, while important, may not fundamentally alter the shelf circulation on shorter than decadal time scales.

Regional analysis reveals a positive onshelf heat and freshwater transport by the ocean in all basins except the Amundsen-Bellingshausen (AB) shelf. Export of High Salinity Shelf Water is the principal cause of these fluxes. The AB shelf, on the other hand, exports freshwater to the ocean, indicating onshelf transport of Circumpolar Deep Water.

1. Introduction

The Antarctic continental shelf extends hundreds of kilometers from the Antarctic coastline with an average depth (~500 m) that is significantly greater than a typical midlatitude continental shelf (~ 100 m) (Fig. 1). Four key subsystems of Earth's climate – the atmosphere, ocean, sea ice, and land ice – interact in this region. Despite its relatively small area, less than 1% percent of the Earth's surface, the Antarctic shelf governs some of the key processes regulating global climate, the ocean meridional overturning circulation, and global sea level.

The Antarctic Ice Sheet (AIS), the largest single mass of freshwater on Earth, sits on the Antarctic continent and floats over the Antarctic continental shelf. In recent decades, the AIS has experienced accelerated loss, particularly in the West AIS (Chen *et al.* 2009; Pritchard *et al.* 2009; Velicogna 2009; Rignot *et al.* 2011; McMillan *et al.* 2014), as well as in the East AIS (Pritchard *et al.* 2012). The discharge of the AIS takes place through its floating extension on the coastal periphery, referred to as the ice shelf. Melting from the bottom of the ice shelf, along with calving of icebergs, is known to be the primary mechanism of the ice shelf mass loss (Depoorter *et al.* 2013; Rignot *et al.* 2013). The ice shelf is very sensitive to external perturbations due to a positive feedback, known as the buttressing effect; mass loss at the front of the shelf can lead to accelerated flow on the upstream glaciers, further accelerating mass loss (De Angelis and Skvarca 2003; Scambos *et al.* 2004; Dupont and Alley 2005; Schoof 2007).

Warm water that contributes to the basal melt of the ice shelf is delivered across the northern boundary of the Antarctic continental shelf, where the shelf sea meets the Southern Ocean. The channel geography of the Southern Ocean and climatological westerly atmospheric wind establishes a deep-reaching eastward flow, the Antarctic Circumpolar Current (ACC), which circles the globe and squeezes through the Drake Passage (56°S – 62°S). Much of the water in the ACC is Circumpolar Deep Water (CDW), a mixture of intermediate and deep waters from all ocean basins with a unique temperature and salinity (roughly 1-2°C and 34.62-34.78 PSU). CDW has two types: Upper CDW (UCDW), marked by a temperature maximum, low oxygen and high nutrient concentrations; and Lower CDW (LCDW), distinguished by a salinity maximum. The location of surfacing of UCDW defines the southern end of the ACC (Orsi *et al.* 1995). Although most of CDW returns to the north at the surface through Ekman transport (Rintoul *et al.* 2001), some floods onto the Antarctic shelf becoming an important source of heat for ice shelf basal melt (mode 2 melting, according to the nomenclature of Jacobs et al. (1992)). Due to the close proximity of CDW to the continental shelf in the Amundsen and Bellingshausen (AB) Seas, warm CDW is able to move across these shelves and into the ice shelf cavity in a mostly unmodified form (T > 0°C). In particular, relatively unmodified CDW has been found near the bottom of multiple sectors across the AB shelf seas (Jacobs *et al.* 2012), including the cavities of Pine Island Glacier (Jacobs *et al.* 1996; Jenkins *et al.* 2010; Jacobs *et al.* 2011), Getz (Jacobs *et al.* 2013), and George VI (Jenkins and Jacobs 2008) ice shelves.

In this study, we use a regional coupled climate model to quantify the heat and freshwater exchange across the Antarctic continental shelf break. Diagnosing the oceanic transport of heat and freshwater onto the shelf is a first step towards constraining estimates of mode 2 melting. To understand the CDW intrusion into the ice shelf cavity, we first need to know the mean and variability of heat and freshwater exchange onto the shelf seas. Despite its importance, quantifying the cross shelf heat and freshwater exchange has proven to be difficult. Observational estimates are hampered by measurements that are both temporally and spatially sparse. Regional modeling efforts have been limited in the sense that they focus on a local area, and the atmosphere is often prescribed (e.g., Thoma *et al.* 2008; Dinniman *et al.* 2011; Hellmer *et al.* 2012). In addition, global coupled ocean-atmosphere models are limited due to biases in atmospheric climatology and low spatial resolution that does not resolve ocean and land topography or ocean mesoscale eddies.

To overcome these hurdles, we use a newly developed regional coupled climate model that is applied to the Southern Ocean and Antarctic continent. The regional domain allows us to use sufficiently high resolution to resolve the small-scale bathymetry that strongly constrains the circulation on the continental shelf. By nudging the upper atmosphere towards reanalysis, we minimize biases in the atmospheric large-scale flow, but still allow for a fully coupled simulation with free development of air-ocean-sea ice interactions. Thus, the model respects energetics and momentum interactions that are lost when atmospheric conditions are prescribed.

We also quantify the heat and freshwater budgets for local shelf seas to explore regional differences in the transport. While the AB shelf is favorable to CDW intrusion due to the nearby ACC, the Ross and Weddell shelves are located a significant distance away from the warm waters of the Southern Ocean. Although both Ross and Weddell gyres transport CDW to the shelf break, it is cooled along the way (e.g., Whitworth *et al.* 2013). These shelves are filled with cold, high salinity water (referred to as High Salinity Shelf Water, HSSW) created through cooling and brine rejection during sea ice formation in coastal polynyas. HSSW is sufficiently dense to flow into the ice shelf cavities. Although at the freezing temperature at the surface, HSSW is able to cause melting under the shelf due to the depression of the freezing point of sea water with depth (mode 1 melting, Jacobs *et al.* (1992)). The ice shelf basal melt forms fresh and sub-freezing waters (Ice Shelf Water) that mix with HSSW and CDW to create dense Antarctic Bottom Water, which is a component of the global thermohaline circulation.

Our focus on the heat and freshwater budgets is motivated by the need to quantify and understand the processes regulating ice shelf basal melt rates. The ice shelves themselves, however, play a role in both heat and freshwater budgets of the continental shelves surrounding the Antarctic Continent; melting ice provides a sink of heat and source of freshwater. The coupled model system used in this study does not include ice shelves explicitly. This lack is common to most current coupled climate models, reflecting the difficulty of incorporating an active ice shelf into a climate model. We estimate the magnitude of the effect that ice shelves could have on heat and freshwater budgets in the context of our results from the coupled model solutions. Although the ice shelf is important for the budgets, we obtain useful flux estimates from our model. Our results provide a benchmark for comparison in future studies where the entire atmosphere-ocean-sea ice-land ice system is fully coupled.

Section 2 describes the model system along with its forcing and initialization. Section 3 presents the details of a novel, tracer-based method that we apply to capture the heat and freshwater transports. Analysis of the heat and freshwater budgets for the entire Antarctic shelf sea, as well as the local shelf seas, are presented in Section 4. The implications of these results are discussed in Section 5 and our conclusions are presented in Section 6.

2. The ACCIMA model

We use a regional coupled modeling system developed by the ACCIMA (Atmosphere-ocean Coupling Causing Ice shelf Melt in Antarctica) project for high southern latitudes that originates from a version of the Regional Arctic System Model (RASM; Maslowski *et al.* 2012; http://www.oc.nps.edu/NAME/name.html; Roberts *et al.* 2015). The four components of the ACCIMA modeling system are (i) Polar-optimized Weather Research and Forecasting model

(PWRF; e.g., Bromwich *et al.* 2009; Bromwich *et al.* 2013) for the atmosphere, (ii) Parallel Ocean Program (POP2; Smith *et al.* 2010) for the ocean, (iii) Community Land Model (CLM; Oleson *et al.* 2010) for land (a different land model from that used in RASM), and (iv) Community Ice CodE model (CICE; Hunke and Lipscomb 2010) for sea ice. These models are coupled through the National Center for Atmospheric Research Community Earth System Model's flux coupler (Craig *et al.* 2012).

These models share a 10,560 km by 10,560 km polar stereographic domain centered over the South Pole. This domain covers the entire Antarctic continent and the bulk of the Southern Ocean, including the key circumpolar oceanic fronts. Two horizontal resolutions are used: 60-km spacing for the atmosphere and land grids, and 10-km spacing for the ocean and sea ice grids. The atmosphere is constrained at the boundaries and in the interior by the European Centre for Medium-Range Weather Forecasts ERA-interim reanalysis (Dee *et al.* 2011). These fields are available every 6 hours but are interpolated to 3 hours for our simulation. Meteorological conditions are imposed along the lateral (closed) boundaries of the atmosphere. For our polar stereographic domain, boundary conditions alone cannot provide sufficient upstream information; so spectral nudging is applied in PWRF throughout the interior of the domain for horizontal wind, temperature, and geopotential height. The nudging is applied only above 300 hPa and for spatial scales larger than wavenumber 7, i.e., > 1500 km, with a time scale of an hour. This nudging technique, implemented by Glisan *et al.* (2012) for the Arctic, constrains the large-scale atmosphere while allowing free evolution of the mesoscale circulation and the interface with the ocean and land.

The ocean model is also closed around the outer boundary. The global overturning circulation is imposed on through nudging over a buffer zone. The ocean lateral boundary temperature and salinity is relaxed toward their monthly climatology from the World Ocean Atlas 2013 (WOA13; Locarnini *et al.* 2013; Zweng *et al.* 2013) in the area north of 50°S. The nudging time scale is 3 months at 45°S and northward, and tapers to infinity between 45°S – 50°S.

Initial conditions are handled carefully because the ocean and land models have relatively long adjustment time scales. The models were first integrated separately to allow them to adjust to initial conditions before they were coupled. The ocean/sea ice and land models are first integrated uncoupled from climatological initial conditions (e.g., WOA13 for the ocean and Qian *et al.* (2006) for the land) forced by a prescribed atmosphere from the version 2 Common Ocean-ice Reference Experiments dataset (Large and Yeager 2008). After these simulations have reached an equilibrium seasonal response, the models are then integrated with coupling for three additional years with the PWRF forced by repeating the ERA-interim conditions for 1999 to allow all of the models to equilibrate.

The simulation used for this study is run from 1999 through 2011, providing 13 years of simulation. The details of how the modeling system performs will be presented in a separate paper. We nonetheless illustrate a few features of the overall performance that are relevant to cross-shelf heat and freshwater transports. The sea ice climatology and variability provide a stiff test for the coupled system because simulating these quantities critically depends on the oceanic stratification and atmospheric radiation and precipitation, which are not well constrained by the lateral boundary conditions or nudging of the upper atmosphere. In addition, sea ice plays an important role for the cross-shelf exchange as discussed earlier. Simulated sea-ice concentration (Fig. 2) compares well to that from the National Snow and Ice Data Center satellite microwave measurements (Meier *et al.* 2013). For February, when sea ice has its minimum extent, climatological sea ice concentration obtained from the 13-yr ACCIMA simulation reasonably captures the observed climatology (from 1999-2011) with large (small) sea ice extent over the Weddell and Ross (AB and East Antarctic) shelves (Figs. 2a,b), although the sea ice in the AB shelf is under-represented in the model. For September, when sea ice has its maximum extent, the Antarctic shelf area is fully covered both in the simulation and observation (Figs. 2c,d).

The ocean volume transport through Drake Passage is 120 ± 11 Sv (1 Sv = 10^6 m^3 s^{-1}), which matches reasonably well with observational based estimates of 134 ± 11 Sv (Cunningham *et al.* 2003) and 141 ± 13 Sv (Koenig *et al.* 2014). Oceanic fronts develop in the ACC at realistic locations. Annual mean precipitation is realistically low over the arid Antarctic continent and increases towards the north over the ocean (not shown).

Antarctic continental shelf areas are defined as ocean areas near the Antarctic coast with depths shallower than 1,000 m (Fig. 1, details in Table 1). Monthly mean total heat content $\overline{H_T}$, where the overbar indicates the monthly time mean, is calculated from the monthly mean ocean temperature, $\overline{T}$, as

$$\overline{H_T}(n) = \sum_j c_p \rho \overline{T}(n,j) \Delta V(j), \quad (1)$$

where n is the time index, j is the model cell index for all cells classified as "shelf", and the sum is over all grid boxes on the continental shelf. Here c_p = 3.996×10^3 J kg^{-1} K^{-1} is the specific heat capacity of seawater. We assume that the seawater density is constant, ρ = 1.020 $\times 10^3$ kg m^{-3}. The grid cell volumes, ΔV, are not functions of time because POP2 is a z-coordinate model with a rigid ocean surface. Similarly, the total salt content $\overline{S_T}$ (kg salt) is calculated from the saved monthly mean salinity, $\overline{S}$, as

$$\overline{S_T}(n)=\sum_j \rho\bar{S}(n,j)\Delta V(j). \quad (2)$$

Total heat content over the length of the simulation (Fig. 3a) shows a clear seasonal cycle, as expected, along with interannual variation in the high and low heat content. There is a 3 to 4 year initial change in the heat content, but it does not seem to have a trend in the last decade. Total salt content (Fig. 3b) also shows a seasonal cycle with increased salt content in the late winter and low salt content in the late summer. After an initial adjustment over the first 4 years, the salt content maintains a constant value, although there is a hint at the end of this simulation of an increasing trend in salt content.

3. Calculating heat and freshwater fluxes

The heat and freshwater content of the shelf seas are regulated by the surface (through air-sea heat exchange, evaporation, precipitation, and sea ice formation/melting), lateral oceanic transport across the shelf break, and melting/freezing on ice shelf sides. In defining the "surface" in this way, we view sea ice as external to the ocean, so that freezing (melting) is a sink (source) of freshwater to the shelf sea, and the transport of heat and freshwater associated with sea ice advection will be counted as part of the atmospheric transport. In the absence of ice shelves, as in our model, the oceanic exchange must balance the surface fluxes in a steady state, as opposed to the three-way balance in the real ocean.

The total heat content change (ΔH_T) of the Antarctic shelf is calculated every month from snapshots of the temperature field obtained at the beginning of two successive months:

$$\Delta H_T(n)=\sum_j c_p\rho\left[T(n+1,j)-T(n,j)\right]\Delta V(j) \; . \quad (3)$$

Because the total content change is the sum of the oceanic and surface exchange, we can use the model diagnosis of the surface heat exchange, ΔH_S, and compute the oceanic heat exchange, ΔH_O, as a residual:

$$\Delta H_O(n) = \Delta H_T(n) - \Delta H_S(n). \tag{4}$$

While this residual method gives us an exact measure of the ocean's heat transport, a limitation is that we obtain only temporal evolution of the oceanic heat exchange, while spatial and vertical structures are unknown.

We adopt an alternative method to compute the oceanic heat exchange using a passive tracer in the ocean model. With this strategy, we calculate the oceanic heat exchange using a passive tracer, C_T, that is re-initialized at the start of each month to the local temperature in each cell, $C_T(n,j) = T(n,j)$. The tracer C_T is advected and diffused by oceanic circulation using the same vertical and horizontal fluxes as for the temperature. However, unlike the temperature field, the tracer C_T has no surface flux; so the difference between the tracer at the end of the month, $C_T(n+1)$, and its value at the start of month, $C_T(n)$, is due purely to oceanic advection and mixing, as if the ocean had an insulating upper boundary. When vertically integrated, the difference is an estimate of the oceanic heat exchange of shelf seas as:

$$\Delta H_O^*(n) = \sum_j c_p \rho \left[C_T(n+1,j) - C_T(n,j) \right] \Delta V(j). \tag{5}$$

The surface heat flux is computed as a residual between the total and the oceanic heat exchanges:

$$\Delta H_S^*(n) = \Delta H_T(n) - \Delta H_O^*(n). \tag{6}$$

Throughout this study the asterisk (*) is used to denote a quantity that is obtained using the tracer method, to differentiate it from the direct residual calculation in (4).

It is important to note that there is a slight mismatch between the tracer-based (ΔH_O^*) and the residual-based (ΔH_O) estimates. The mismatch occurs because diabatic processes (primarily the surface exchange) over the course of the month long cycle lead to changes in temperature. So even though the tracer is exchanged across the shelf break by the same velocity as the temperature, their gradients will differ slightly, leading to different estimates of oceanic advection and diffusion compared to the temperature. Nonetheless, we find the mismatch remains small relative to the oceanic flux (shown below), so that the tracer method provides a useful estimate.

We can perform a similar calculation for the freshwater flux. The total salt content change on the Antarctic shelf is obtained from the salinity field at the beginning and the end of each month. It remains to convert the salt content change to an equivalent freshwater volume change. Using an ocean reference salinity, S_{ref} = 34.7 g kg^{-1}, and a freshwater density, ρ_{fw} = 10^3 kg m^{-3}, the total freshwater flux [kg month^{-1}] for the Antarctic shelf sea is

$$\Delta F_T(n) = -\sum_j \left[S(n+1,j) - S(n,j) \right] \Delta V(j) \cdot \rho_{fw} / S_{ref} \ . \tag{7}$$

The oceanic freshwater exchange (ΔF_O^*) is obtained with a passive tracer, C_S ,

$$\Delta F_O^*(n) = -\sum_j \left[C_S(n+1,j) - C_S(n,j) \right] \Delta V(j) \cdot \rho_{fw} / S_{ref} \ , \tag{8}$$

where C_S is reset to the salinity at each grid point at the beginning of each month. The residual surface freshwater exchange (ΔF_S^*) is

$$\Delta F_S^*(n) = \Delta F_T(n) - \Delta F_O^*(n) \ . \tag{9}$$

The above equations quantify the heat and freshwater fluxes for the entire volume of shelf water. To facilitate comparison with atmospheric flux, we convert these quantities to surface equivalent fluxes [W m^{-2} for heat flux and mm day^{-1} for precipitation] by dividing them by the shelf area and converting time units.

To validate the new tracer-based methodology, we compare the two estimates of the oceanic heat exchange; one based on the tracer as in Eq. (5) and the other obtained as a residual as in Eq. (4). The tracer-based oceanic heat exchange (black curve in Fig. 4a) matches well with that of the residual method (red curve in Fig. 4a), although the former is systematically greater (smaller) in March-May (December-January) than the latter (blue curves in Figs. 4a,b). This is probably because during summer (fall), the offshelf region gains (loses) surface heat more rapidly than the onshelf region due to more ice cover over the shelf, changing the cross-shelf temperature gradient compared to the tracer gradient. Nonetheless, the difference remains a factor of 10 smaller than the two flux estimates except for January, May, and June, when the oceanic heat exchange is small. The root-mean-square error of these heat flux estimates is about 3.1 W m^{-2} for all months.

The two estimates of freshwater flux also match well, despite a similar systematic bias. The tracer-based freshwater oceanic exchange (black curve in Fig. 4c) is less (greater) than that of the residual method (red in Fig. 4c) during December to April (July to October) (see blue curves in Figs. 4c,d for the difference). The explanation for the seasonal pattern in the difference is related to the difference in the sea ice growth/melt over the ocean vs. the shelf leading to differences in onshelf freshwater transport vs. onshelf tracer transport. The root-mean-square error for the freshwater flux is 0.7 mm day^{-1} for all months. Based on this favorable comparison and the benefit explained below, we will use the tracer-based estimate for the oceanic exchange of both heat and freshwater.

The tracer-based method allows analysis of spatial structures of the oceanic exchange. To examine the vertical structure, we integrate the tracer equations (Eqs. 5 and 8) from 300 m (at the base of the main pycnocline), being deep enough to avoid direct influence of the surface fluxes, to the bottom. This quantity includes the tracer content change both in the lateral direction across the shelf break and in the vertical direction across the 300 m surface. Vertical exchange at 300 m can occur through vertical diffusion and advection, both of which are available from the model output. By subtracting the vertical exchange from the tracer content change between 300 m and below, purely lateral tracer mixing at that layer can be retrieved. To further investigate the entire vertical structure of the oceanic fluxes, we repeat the above process from each model grid depth to the bottom.

The horizontal variation of these changes is obtained by integrating Eqs. (5) and (8) over an area of interest, e.g., over the AB shelf sea (red shading in Fig. 1). Such local calculations include the inter-shelf (alongshore) flux between adjacent shelf areas; but we assume that the flux between the shelves is small relative to the oceanic flux at the shelf break. This assumption is based on the fact that the climatological inter-shelf temperature gradient is small relative to the cross shelf temperature gradient. In addition, the boundary area between shelves is far smaller than the boundary area at the shelf break.

4. Results

A detailed understanding of the fluxes of heat and freshwater on the Antarctic continental shelf has proved elusive due to the dearth of observations and concerns about the fitness of global climate models. We use our 13-year integration of the ACCIMA model to establish the roles of the atmosphere, sea ice, and ocean in regulating the shelf waters. In particular, how large is the net heat transport, relative to the fluxes required to melt ice in the Antarctic ice shelves? The annual cycle and the time mean of the fluxes for the whole shelf are discussed first, followed by an analysis of their vertical structure. We then look at the anomaly of these fluxes from the average seasonal variation to detect trends. Finally, we analyze results for the four subregions indicated in Fig. 1.

(a) Monthly and seasonal exchange for the whole Antarctic Shelf

The overall heat content change for the entire Antarctic shelf sea (Fig. 5a) displays a large seasonal cycle with a range of 200 W m^{-2}. Monthly total heat content change (black curve; ΔH_T in Eq. (3)) is compressed into austral summer and fall, with strong heating during the summer and cooling during fall and early winter. Most of the change takes place through the surface heat flux (blue curve; ΔH_S^* in Eq. (6)) between the ocean and either the atmosphere (mainly) or the sea ice. The annual cycle of the oceanic heat exchange (red curve; ΔH_O^* in Eq. (5)) vacillates roughly between 5 and 30 W m^{-2} explaining 10-40% of the total heat content change, depending on the season. The maximum oceanic heat gain peaks around March (red curve in Fig. 5b), which is about two months after the surface heating maximum (blue curve in Fig. 5b). The maximum oceanic heat exchange is concurrent with the maximum of the total heat content itself (but not the total heat content change, which is dominated by the atmosphere; Fig. 3), as well as the minimum of sea ice concentration over the shelf sea (not shown), indicating that heating of the shelf by oceanic flux is compensated by exchange of heat to the atmosphere and sea ice. The minimum of the oceanic heat exchange tends to spread from May to December, at times that the shelf is mostly covered by the sea ice. This annual cycle of the oceanic transport will be discussed later in this section.

The freshwater content change on the Antarctic shelf sea is similarly examined (Figs. 5c,d). The surface freshwater flux (blue curve in Fig. 5c; ΔF_S^* in Eq. (9)) plays a key role in the total freshwater content change (black curve in Fig. 5c; ΔF_T in Eq. (7)), with an annual cycle of about ±10 mm day^{-1}. The maximum of the surface freshwater flux (negative salt flux) takes place during the summer, when sea ice melts. From April to October, sea ice formation and, hence, brine rejection leads to a negative freshwater flux (positive salt flux). The oceanic freshwater exchange (red curve in Fig. 5c; ΔF_O^* in Eq. (8)) shows a sharp increase centered in March, delayed by two months from the total freshwater exchange maximum, as for the oceanic heat exchange. This strongest offshelf oceanic exchange coincides with the highest total freshwater content (not the total freshwater content change) in the shelf sea.

(b) Anomaly exchange for the whole Antarctic Shelf

We now remove the seasonal cycle (Figs. 5b,d) from the heat and freshwater content change time series (Figs. 5a,c) to examine the interannual heat and freshwater fluxes (Fig. 6). The total heat content change time series (black curve in Fig. 6a) is well matched by the surface heat flux (blue curve in Fig. 6a), while the match with the oceanic heat flux (red curve in Fig. 6a) is close only when the surface heat flux is near zero. This indicates that the interannual variability of the total heat content change is largely attributed to the changing surface heat flux; the contribution from the oceanic heat flux is relatively small. The correlation between the total heat content change and the surface heat flux is 0.88 while the correlation with the oceanic flux is 0.38.

This is not the case for the freshwater flux. The oceanic freshwater flux (red curve in Fig. 6b) matches reasonably well with the total freshwater content change (black curve in Fig. 6b), although the contribution of the surface freshwater flux (blue curve in Fig. 6b) to the total is also important. The correlation of the oceanic freshwater flux with the total freshwater flux is 0.85 while the correlation of the surface flux is 0.71.

(c) Long term mean exchange for the whole Antarctic Shelf

The time mean budget of heat and freshwater fluxes for the whole Antarctic shelf (Fig. 7) shows that the ocean adds heat and freshwater to the shelf which goes to the atmosphere and sea ice. Despite a relatively small annual cycle, the oceanic heat transport remains positive most of the time, with its time mean value of about 12.2 W m^{-2}. The standard deviation (4.1 W m^{-2}) of the time series with the seasonal cycle and linear trend removed is shown to indicate a measure of uncertainty for the time mean value. By multiplying the total area of the shelf sea this number can be translated to the total oceanic heat transport for the entire Antarctic shelf sea, 0.034 PW. This contrasts to the surface heat flux that varies greatly over a year from a positive to a negative value, but mostly cancels having a time mean value of 12.5 W m^{-2} (or 0.035 PW for the entire Antarctic shelf sea). The standard deviation for the surface heat flux after the seasonal cycle and linear trend is removed (8.4 W m^{-2}) is comparable to the time mean. The above results suggest that for the time mean, the oceanic exchange is an important way to bring heat from the Southern Ocean into the shelf sea (red arrows in Fig. 7), while the atmosphere and sea ice remove the heat from the shelf sea. However, the direction of heat exchange is contingent upon the sign of the surface heat exchange.

For the freshwater budget (blue in Fig. 7), the time mean oceanic exchange is also positive (1.0 mm day^{-1}), with an interannual standard deviation of 0.9 mm day^{-1}. The amplitude of the annual cycle of the freshwater flux is roughly 3.0 mm day^{-1}. On the other hand, the time mean surface freshwater flux (1.3 mm day^{-1}) is an order of magnitude smaller than the peak surface fluxes, which shows the dominance of the seasonal cycle. The standard deviations of the surface fluxes without its seasonal cycle and linear trend is 0.7 mm day^{-1}. The net onshelf oceanic transport of freshwater reveals that for the entire Antarctic shelf sea, the salinity loss due to the export of the HSSW off the shelf contributes more than that from the import of salinity through the CDW onto the shelf. It will be shown later that this competition varies by the location, and in the AB seas in particular, the CDW import leads to a negative oceanic freshwater flux. The surface freshwater exchange is positive (to the atmosphere), showing that the contributions from the freezing of sea ice and evaporation are greater than that from the melting of sea ice and precipitation.

It is important to note that the bulk of the ocean heat exchange (more than 90%) occurs above the main pycnocline (300 m). The small amount of heat added to the lower ocean layer moves to the upper layer and then to the atmosphere. In contrast, the onshore freshwater flux is about evenly split between the upper and lower layers. Again, the freshwater flux to the lower layer moves upward to the surface layer and then to the atmosphere and sea ice.

(d) Depth and seasonal variation exchange for the whole Antarctic Shelf

The total heat content change integrated over the whole shelf and over depth intervals starting from the bottom (Fig. 8a) exhibits two different regimes with depth. The upper layer from the surface to ~300 m shows a clear annual cycle of warming in the summer and cooling in the fall and winter, both penetrating downward with a time scale of a few months. This penetration is dominated by a combination of the surface heat exchange with atmosphere and sea ice (Fig. 8d) and vertical mixing of the ocean below (Fig. 8c), and is due to the fall and winter deepening of the surface mixed layer and vertical convection due to surface density increases, which is primarily attributed to sea ice formation and brine rejection. The lateral heat exchange (Fig. 8b) is mostly positive throughout the year in this upper layer, which helps the downward expansion of the warm anomaly in late summer, but opposes that of the cold anomaly during the winter. Below 300 m, the annual cycle is decoupled from the layers above it. The total heat content change (Fig. 8a) has a much smaller annual cycle than in the upper layer. This is consistent with the difference in annual cycle amplitude between the surface and the oceanic heat exchange (Fig. 5b). Also, in this lower layer, most of the total heat content change (Fig. 8a) is explained by the lateral heat exchange (Fig. 8b), which brings heat onto the shelf in the summer, and removes it in fall. While driven by the ocean, this lateral heat flux is remarkably in phase with surface fluxes.

The annual cycle of the freshwater flux is largely a balance between two opposing tendencies: vertical transport removes freshwater to offset brine rejection and freshwater transport by ice drifting at the surface (Fig. 8g). The ocean continually brings in freshwater through the export of HSSW (Fig. 8f). The freshwater budgets of the shallow and deep layers are more closely connected due to the weaker freshwater flux at the surface and the deep convection created by winter sea ice freezing. The surface freshwater flux (Fig. 8h) dominates the total freshwater content change (Fig. 8e) at the surface, but slightly below, the lateral and vertical mixing of the ocean is important. For example, in April to October relatively salty water, i.e., negative freshwater flux anomaly, is formed at the surface (Fig. 8h). The vertical mixing of the ocean transports the salty water downward (Fig. 8g), while the lateral exchange (Fig. 8f) constantly takes the salty water off the shelf.

(e) Long term mean exchange for four shelf subareas

We now repeat the heat and freshwater budget analysis for each of the regional areas (Fig. 9). First, as for the entire Antarctic shelf sea, the time mean oceanic fluxes reveal that the ocean brings heat and freshwater onto the shelf seas for three local shelf seas, but not the AB shelf sea.

However, for these three shelf seas, the amount of the oceanic transports greatly varies. For instance, the time mean oceanic heat exchange for the East Antarctic shelf sea (Fig. 9d) is about twice and twenty times larger than those for the Ross (Fig. 9a) and Weddell (Fig. 9c) shelf seas, respectively. The inter-shelf differences can be also seen for the freshwater flux. These differences are ultimately coupled to the time mean surface flux, which, for a steady state, balances the input by the oceanic flux. Secondly, two distinct layers of annual cycle can be seen for the Ross and East Antarctic shelf seas, while vertical differences are not clear for the Weddell.

Unlike the other shelf seas, the AB shelf sea has a time mean negative freshwater flux. This is consistent with the fact that the southern side of the ACC only flows along the AB shelf break and can deliver CDW onto the shelf in relatively unmodified form (Jacobs *et al.* 2012). Because the CDW is warm and salty, its intrusion contributes to a negative freshwater flux. For the other shelf seas, the export of the HSSW appears to be more important, and the offshelf cold and salty water transport leads to a positive heat and freshwater flux to the shelf seas.

5. Discussion

The total heat and freshwater budgets can be compared to the total ice shelf basal melt. Observation-based estimates of the total ice shelf melt around the Antarctic range from 750-1,450 Gt per year (Jacobs *et al.* 1996; Depoorter *et al.* 2013; Rignot *et al.* 2013). This amount corresponds to roughly 0.01 PW (or an average 5 W m^{-2} over the whole shelf) of heat consumption and 2 mm day^{-1} of freshwater input. These values are comparable to the time mean heat and freshwater fluxes from the Southern Ocean (Fig. 7). Despite the dominance of the atmosphere in the annual cycle, the results suggest that the oceanic transport is responsible for bringing the heat energy needed to melt the ice shelf. Otherwise the shelf seas would cool and freshen in response to the atmospheric driving, which would in turn reduce the melting rates. The heat needed to melt the ice shelves is about the same size as the non-seasonal heat flux (Fig. 6) and is about a quarter of the peak surface heat flux.

If the model had ice shelves, they could have had a strong effect on the simulation results. The initial impact would be a cooling and freshening of the shelf seas, which would in turn impact the surface fluxes to the atmosphere and lateral fluxes to the oceans. The atmospheric response is perhaps easier to predict: cooler surface temperatures would reduce the heat flux to the atmosphere, cooling the coastal regions, and potentially reducing precipitation, as part of the flux is in latent heat. Naively, one would expect the oceanic heat flux to increase, given the increase in the temperature gradient between the Southern Ocean and the (now colder) shelf seas. However, if freshening reduces the formation and export of HSSW, the oceanic response might be muted, or even the opposite sign. Indeed, preliminary simulations using an ocean-sea ice-ice shelf model (but without a coupled atmosphere) suggest that the oceanic heat exchange decreases with the ice shelf thermodynamics active (not shown).

From another point of view, all of the heat gained by the shelf waters eventually moves to the atmosphere in a steady state (and there is no long-term trend in the temperature of the shelf waters, Fig. 3). In a coupled calculation, the heat not absorbed by melting the ice shelves thus goes to the atmosphere, changing its structure and circulation. The real impact of including ice shelves in the model may be most significant on the lower atmosphere around the coast.

The freshwater produced by a melting ice shelf is comparable to the interannual variation in freshwater flux (Fig. 6) and is about a quarter of the peak freshwater flux. The lack of ice shelves in this model should lead to saltier HSSW, or could be compensated by a reduced export of sea ice.

Ice shelf melt will certainly influence the coastal ocean around Antarctica, but this model study suggests the size of these effects may be modest and can be accounted for by small changes in the ocean exchange with the atmosphere or lateral ocean exchange across the shelf break. The modeled magnitude of atmospheric and oceanic fluxes are sufficiently large that freshwater and heat fluxes associated with ice melt, while important, will not radically alter the shelf circulation. Further research is clearly merited, and but we believe that the estimates in Fig. 7 are a valuable step toward the complete shelf sea heat and freshwater budget.

6. Conclusions

Analysis of a coupled ocean-atmosphere simulation shows that surface exchange, which we define to include both atmosphere and sea ice, explains the bulk of the annual cycle in the total content change for both heat and freshwater on the Antarctic shelf. The annual cycle in surface heat and freshwater exchange amplitude is on the order of 100 W m^{-2} and 10 mm day^{-1}, respectively, when averaged over the entire shelf. The amplitude of the annual cycle in oceanic exchange is just 1/5 as large and exhibits a compressed seasonal cycle, concentrated in the sea ice-free season of the shelf seas from December to May. While the surface exchange changes greatly throughout the year, oceanic transport is more stable and nearly always positive, bringing both heat and freshwater onto the shelf. In a steady climate, the annual mean transports of the ocean and atmosphere must balance. In the time mean, the atmosphere and sea ice remove heat and freshwater from the shelf seas, which is replenished by the ocean. These net transports are of order 10 W m^{-2} and 1 mm day^{-1}, an order of magnitude smaller than the annual cycle in surface exchanges, but of comparable amplitude to fluctuations in the ocean transports.

Analysis of the vertical structure of heat changes shows two distinct annual cycles in the Antarctic shelf sea temperatures, one above the pycnocline (0-300 m) and the other below (300 m and below). Processes in the upper layer are associated with the atmosphere and sea ice. Temperatures at the surface vary synchronously with the surface fluxes, but lag behind at lower levels. The delay reaches a maximum near 300 meters, where the signal is nearly three months out of phase. Thus, the maximum in the annual cycle at this level occurs in April, at which time the surface has already cooled substantially with the approach of the austral winter. This delay is likely due to the fall deepening of the surface mixed layer bringing warmer water to depth. In contrast, below 300 m, the annual cycle is decoupled from the layers above, and governed almost exclusively by fluctuations in oceanic transport. Temperatures at depth are more in phase with surface annual cycle than at intermediate depths; the maximum appears in December, shortly followed by a minimum in April. Hence, the annual maximum at 300 m coincides with the annual minimum at 600 m.

Overall, the ocean brings both heat and freshwater onto most parts of the shelf except the Amundsen-Bellingshausen (AB) shelf where the freshwater transport reverses sign; the ocean is still a source of heat, but exports freshwater. The AB shelf break is close to the ACC, so that the flooding of warm and salty Circumpolar Deep Water (CDW) onto the shelf can bring both heat and salt. In contrast, the ocean is a significant source of freshwater in the Ross and Weddell shelf seas, the former in particular. Here the drainage of cold, High Salinity Shelf Water (HSSW), which is formed through brine rejection during sea ice growth, leads to a net import of both heat and freshwater onto the shelf. East Antarctica has competition between both processes: at upper levels the ocean serves as a net source of heat and sink of freshwater, consistent with the import of CDW. A net source of freshwater at lower levels is associated with HSSW export; however, it is more than sufficient to compensate for the sink in the upper layer.

Finally, we have developed a new methodology for tracking heat and freshwater content changes in the Antarctic shelf seas. The technique uses two passive tracers to exclude the impact of diabatic processes at the surface. Thus, it quantifies the oceanic transport of heat and freshwater across the shelf break as if the ocean were completely isolated from the atmosphere. Compared to the standard residual method, the tracer method provides additional information on vertical and spatial structure of the oceanic exchange: the tracer-based oceanic heat (freshwater) transport across the entire Antarctic shelf break captures the overall variability of the residual method, but systematically overestimates (underestimates) values during fall by about 10%. This difference arises from the exchanges of heat and freshwater with the surface over the course of analysis cycle, which are in turn transported across the shelf break by the ocean. In addition to providing information on the structure of the transport, the new method bypasses the numerically challenging calculation of cross shelf exchange along complex shelf break geometry. This method can be easily implemented into climate models with any horizontal grid type for multi-model comparison on the cross shelf exchange.

Acknowledgements

This research is supported by NSF Grants ANT-1048989, ANT-1049081, ANT-1049089, and AGS-1264195. We gratefully appreciate this support. We would like to acknowledge the use of computational resources (ark:/85065/d7wd3xhc) at the NCAR-Wyoming Supercomputing Center provided by the National Science Foundation and the State of Wyoming, and supported by NCAR's Computational and Information Systems Laboratory. We thank Tony Craig and

John Cassano for supplying the RASM code and helpful comments. We also thank Ruby Leung for helpful comments. Contribution XXXX of Byrd Polar and Climate Research Center.

References

Bromwich, D. H., F. O. Otieno, K. M. Hines, K. W. Manning, and E. Shilo, 2013: Comprehensive evaluation of Polar Weather Research and Forecasting model performance in the Antarctic. *J. Geophys. Res. Atmos.*, **118,** 274-292, doi: 10.1029/2012JD018139.

Bromwich, D. H., K. M. Hines, and L.-S. Bai, 2009: Development and testing of Polar Weather Research and Forecasting model: 2. Arctic Ocean. *J. Geophys. Res. Atmos.*, **114,** D08122, doi: 10.1029/2008JD010300.

Chen, J. L., C. R. Wilson, D. Blankenship, and B. D. Tapley, 2009: Accelerated Antarctic ice loss from satellite gravity measurements. *Nature Geosci.*, **2,** 859-862, doi: 10.1038/ngeo694.

Craig, A. P., M. Vertenstein, and R. Jacob, 2012: A new flexible coupler for earth system modeling developed for CCSM4 and CESM1. *Int. J. High Perf. Computing Appl.*, **26,** 31-42, doi:10.1177/109434201142814.

Cunningham, S. A., S. G. Alderson, B. A. King, and M. A. Brandon, 2003: Transport and variability of the Antarctic Circumpolar Current in Drake Passage. *J. Geophys. Res. Oceans.*, **108,** 8084, doi: 10.1029/2001JC001147.

De Angelis, H., and P. Skvarca, 2003: Glacier surge after ice shelf collapse. *Science*, **299,** 1560-1562, doi: 10.1126/science.1077987.

Dee, D. P., and Coauthors, 2011: The ERA-Interim reanalysis: configuration and performance of the data assimilation system. *Quart. J. Roy. Met. Soc.*, **137,** 553-597, doi: 10.1002/qj.828.

Depoorter, M. A., J. L. Bamber, J. A. Griggs, J. T. M. Lenaerts, S. R. M. Ligtenberg, M. R. van den Broeke, and G. Moholdt, 2013: Calving fluxes and basal melt rates of Antarctic ice shelves. *Nature*, **502,** 89-92, doi: 10.1038/nature12567.

Dinniman, M. S., J. M. Klinck, and W. O. Smith Jr, 2011: A model study of Circumpolar Deep Water on the West Antarctic Peninsula and Ross Sea continental shelves. *Deep-Sea Research II*, **58,** 1508-1523, doi: 10.1016/j.dsr2.2010.11.013.

Dupont, T. K., and R. B. Alley, 2005: Assessment of the importance of ice-shelf buttressing to ice-sheet flow. *Geophys. Res. Lett.*, **32,** L04503, doi: 10.1029/2004GL022024.

Glisan, J. M., W. J. Gutowski, J. J. Cassano, and M. E. Higgins, 2012: Effects of spectral nudging in WRF on Arctic temperature and precipitation simulations. *J. Climate*, **26,** 3985-3999, doi: 10.1175/JCLI-D-12-00318.1.

Hellmer, H. H., F. Kauker, R. Timmermann, J. Determann, and J. Rae, 2012: Twenty-first-century warming of a large Antarctic ice-shelf cavity by a redirected coastal current. *Nature*, **485,** 225-228, doi: 10.1038/nature11064.

Hunke, E., and W. Lipscomb, 2010: CICE: the Los Alamos sea ice model, documentation and software user's manual, Version 4.1. *Los Alamos National Laboratory Tech. Rep. LA-CC-06-012*, 76pp.

Jacobs, S., C. Giulivi, P. Dutrieux, E. Rignot, F. Nitsche, and J. Mouginot, 2013: Getz Ice Shelf melting response to changes in ocean forcing. *J. Geophys. Res. Oceans.*, **118,** 4152-4168, doi: 10.1002/jgrc.20298.

Jacobs, S., H. Hellmer, C. Doake, A. Jenkins, and R. Frolich, 1992: Melting of ice shelves and the mass balance of Antarctica. *J. Glaciol.*, **38,** 375-387.

Jacobs, S. S., A. Jenkins, H. H. Hellmer, C. F. Giulivi, B. H. Nitsche, and R. Guerrero, 2012: The Admundsen Sea and the Antarctic Ice Sheet. *Oceanography*, **25,** 154-163, doi: 10.5670/oceanog.2012.90.

Jacobs, S. S., A. Jenkins, C. F. Giulivi, and P. Dutrieux, 2011: Stronger ocean circulation and increased melting under Pine Island Glacier ice shelf. *Nature Geosci.*, **4,** 519-523, doi: 10.1038/ngeo1188.

Jacobs, S. S., H. H. Hellmer, and A. Jenkins, 1996: Antarctic Ice Sheet melting in the southeast Pacific. *Geophys. Res. Lett.*, **23,** 957-960, doi: 10.1029/96gl00723.

Jenkins, A., P. Dutrieux, S. S. Jacobs, S. D. McPhail, J. R. Perrett, A. T. Webb, and D. White, 2010: Observations beneath Pine Island Glacier in West Antarctica and implications for its retreat. *Nature Geosci.*, **3,** 468-472, doi: 10.1038/ngeo890.

Jenkins, A., and S. Jacobs, 2008: Circulation and melting beneath George VI Ice Shelf, Antarctica. *J. Geophys. Res. Oceans.*, **113,** C04013, doi: 10.1029/2007JC004449.

Koenig, Z., C. Provost, R. Ferrari, N. Sennéchael, and M.-H. Rio, 2014: Volume transport of the Antarctic Circumpolar Current: Production and validation of a 20 year long time series obtained from in situ and satellite observations. *J. Geophys. Res. Oceans.*, **119,** 5407-5433, doi: 10.1002/2014JC009966.

Large, W., and S. Yeager, 2008: The global climatology of an interannually varying air-sea flux data set. *Climate Dynam.*, **33,** 341-364, doi: 10.1007/s00382-008-0441-3.

Locarnini, R. A., and Coauthors, 2013: *World Ocean Atlas 2013, Volume 1: Temperature.* S. Levitus, Ed., A. Mishonov Technical Ed., NOAA Atlas NESDIS 73, 40 pp.

Maslowski, W., J. Clement Kinney, M. Higgins, and A. Roberts, 2012: The Future of Arctic Sea Ice. *Annu. Rev. Earth Planet. Sci.*, **40,** 625-654, doi: 10.1146/annurev-earth-042711-105345.

McMillan, M., and Coauthors, 2014: Increased ice losses from Antarctica detected by CryoSat-2. *Geophys. Res. Lett.*, **41,** 2014GL060111, doi: 10.1002/2014GL060111.

Meier, W., F. Fetterer, M. Savoie, S. Mallory, R. Duerr, and J. Stroeve, 2013: *NOAA/NSIDC Climate Data Record of Passive Microwave Sea Ice Concentration. Version 2.*, National Snow and Ice Data Center, Boulder, Colorado USA.

Oleson, K. W., and Coauthors, 2010: Technical Description of version 4.0 of the Community Land Model (CLM). *NCAR Tech. Note NCAR/TN-478+STR***,** 267pp.

Orsi, A. H., T. Whitworth Iii, and W. D. Nowlin Jr, 1995: On the meridional extent and fronts of the Antarctic Circumpolar Current. *Deep-Sea Research I*, **42,** 641-673, doi: 10.1016/0967-0637(95)00021-w.

Pritchard, H. D., S. R. M. Ligtenberg, H. A. Fricker, D. G. Vaughan, M. R. van den Broeke, and L. Padman, 2012: Antarctic ice-sheet loss driven by basal melting of ice shelves. *Nature*, **484,** 502-505, doi: 10.1038/nature10968.

Pritchard, H. D., R. J. Arthern, D. G. Vaughan, and L. A. Edwards, 2009: Extensive dynamic thinning on the margins of the Greenland and Antarctic ice sheets. *Nature*, **461,** 971-975, doi: 10.1038/nature08471.

Qian, T., A. Dai, K. E. Trenberth, and K. W. Oleson, 2006: Simulation of Global Land Surface Conditions from 1948 to 2004. Part I: Forcing Data and Evaluations. *J. Hydrometeor.*, **7,** 953-975, 10.1175/JHM540.1.

Rignot, E., S. Jacobs, J. Mouginot, and B. Scheuchl, 2013: Ice-Shelf Melting Around Antarctica. *Science*, **341,** 266-270, doi: 10.1126/science.1235798.

Rignot, E., I. Velicogna, M. R. van den Broeke, A. Monaghan, and J. T. M. Lenaerts, 2011: Acceleration of the contribution of the Greenland and Antarctic ice sheets to sea level rise. *Geophys. Res. Lett.*, **38,** L05503, doi: 10.1029/2011GL046583.

Rintoul, S. R., C. W. Hughes, and D. Olbers, 2001: The Antarctic Circumpolar Current System. *Ocean Circulation and Climate*, G. Siedler, J. Church, and J. Gould, Eds., Academic Press, 271-302.

Roberts, A., and Coauthors, 2015: A case study of high frequency ice-ocean-atmosphere dynamic coupling in the Regional Arctic System Model. *Ann. Glaciol.*, **in press.**

Scambos, T. A., J. A. Bohlander, C. A. Shuman, and P. Skvarca, 2004: Glacier acceleration and thinning after ice shelf collapse in the Larsen B embayment, Antarctica. *Geophys. Res. Lett.*, **31,** L18402, doi: 10.1029/2004GL020670.

Schoof, C., 2007: Ice sheet grounding line dynamics: Steady states, stability, and hysteresis. *J. Geophys. Res. Earth Surf.*, **112,** F03S28, doi: 10.1029/2006JF000664.

Smith, R., and Coauthors, 2010: The parallel ocean program (POP) reference manual: ocean component of the community climate system model (CCSM). *Los Alamos National Laboratory, LAUR-10-01853***,** 144pp.

Thoma, M., A. Jenkins, D. Holland, and S. Jacobs, 2008: Modelling Circumpolar Deep Water intrusions on the Amundsen Sea continental shelf, Antarctica. *Geophys. Res. Lett.*, **35,** L18602, doi: 10.1029/2008gl034939.

Velicogna, I., 2009: Increasing rates of ice mass loss from the Greenland and Antarctic ice sheets revealed by GRACE. *Geophys. Res. Lett.*, **36,** L19503, doi: 10.1029/2009GL040222.

Whitworth, T., A. H. Orsi, S. J. Kim, W. D. Nowlin, and R. A. Locarnini, 2013: Water Masses and Mixing Near the Antarctic Slope Front. *Ocean, Ice, and Atmosphere: Interactions at the Antarctic Continental Margin*, American Geophysical Union, 1-27.

Zweng, M. M., and Coauthors, 2013: *World Ocean Atlas 2013, Volume 2: Salinity.* S. Levitus, Ed., A. Mishonov Technical Ed., NOAA Atlas NESDIS 74, 39 pp.

List of Tables

Table 1: The surface area and the volume for the whole Antarctic shelf and four subareas shown in Fig. 1.

	Ross	AB	Weddell	East	All
Surface area (10^6 km^2)	0.53	0.79	0.67	0.82	2.81
Volume (10^6 km^3)	0.29	0.41	0.35	0.40	1.45

Table 2: Linear trend and standard deviation of the monthly oceanic heat and freshwater content changes for the whole Antarctic shelf and four subareas. The standard deviation is obtained after the seasonal cycle and linear trend are removed. Monthly changes are in units of surface heat flux (W m^{-2}) and surface precipitation (mm day^{-1}). Units for the trends are W m^{-2} $month^{-1}$ and mm day^{-1} $month^{-1}$ for the heat and freshwater fluxes, respectively.

	Ross	AB	Wedd.	East	All
Heat Trend (W m^{-2} $month^{-1}$)	0.059	0.050	0.007	0.039	0.038
Heat Stddev. (W m^{-2})	7.8	7.2	3.2	7.7	4.1
FW Trend (mm day^{-1} $month^{-1}$)	-0.001	0.002	0.006	-0.004	5.e-4
FW Stddev. (mm day^{-1})	1.41	1.37	1.12	2.01	0.91

List of Figures

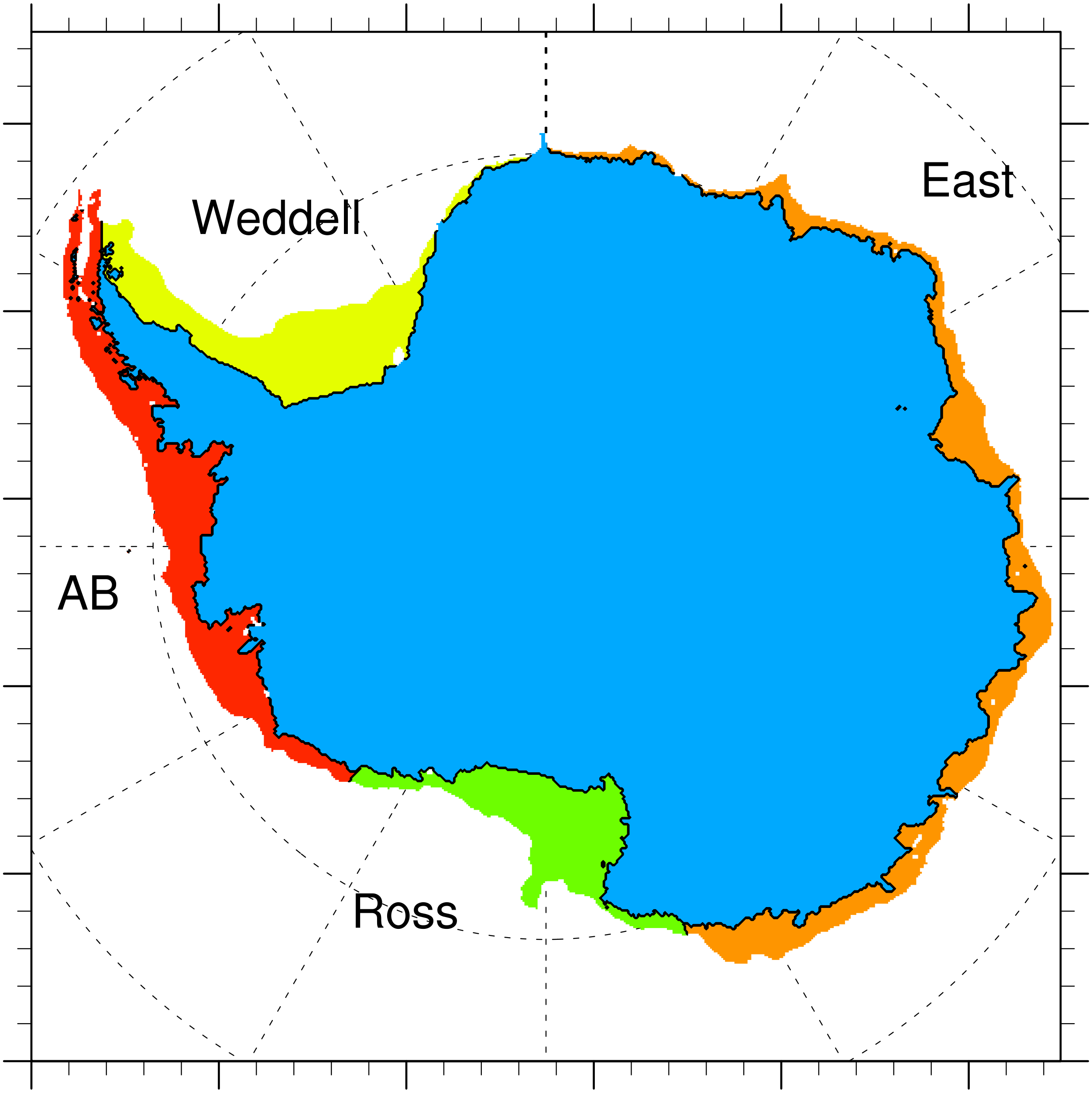

Figure 1: Antarctic continental shelves defined by the depth less than 1 km. The shelves are divided in to four regions: Ross Sea (green), Amundsen-Bellingshausen Seas (red), Weddell Sea (yellow), and East Antarctica (orange) shelves.

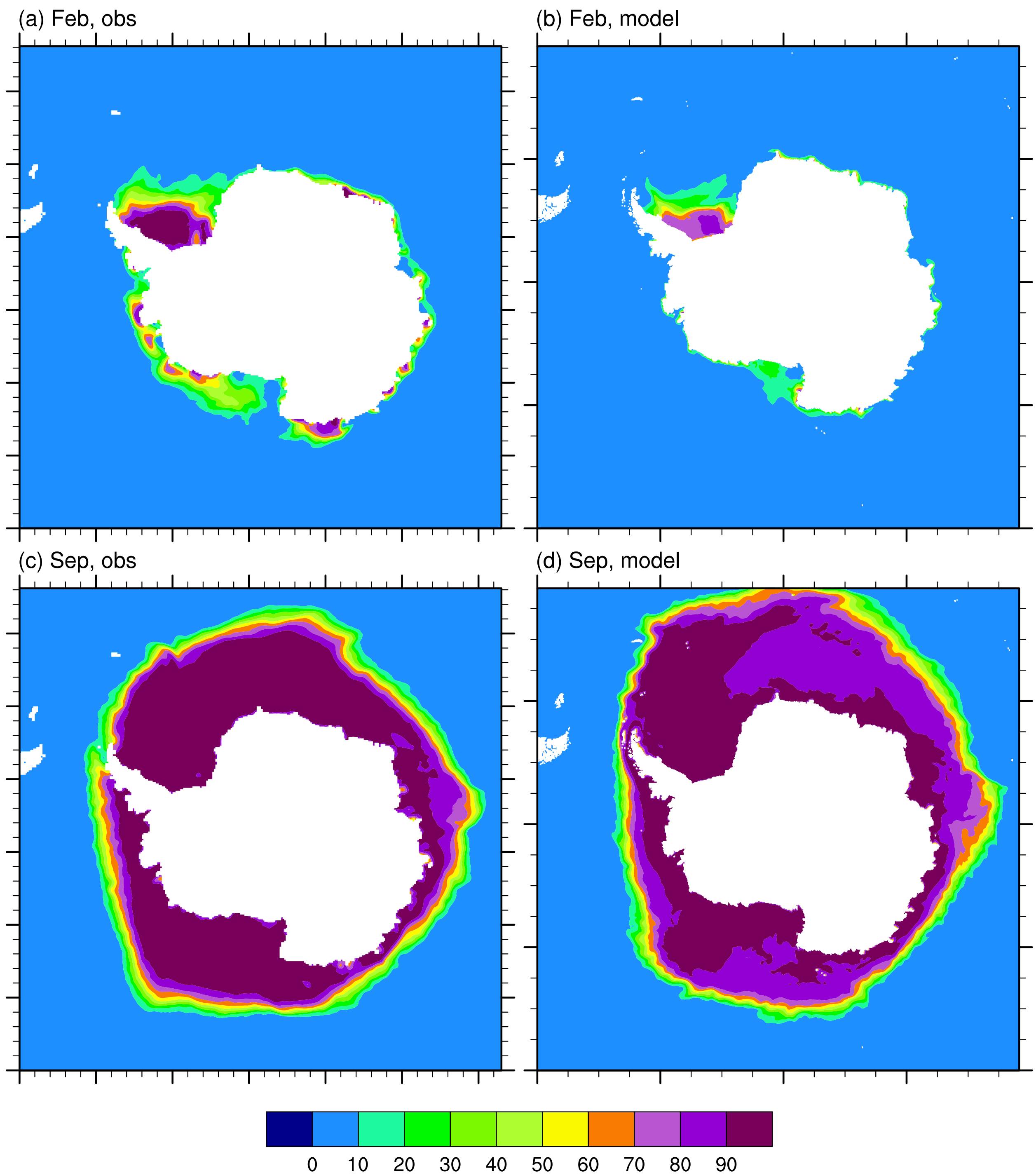

Figure 2: Sea ice concentration climatology (1999-2011) of observation (panels a, c) and our simulation (b, d) for February (panels a, b) and September (panels c, d).

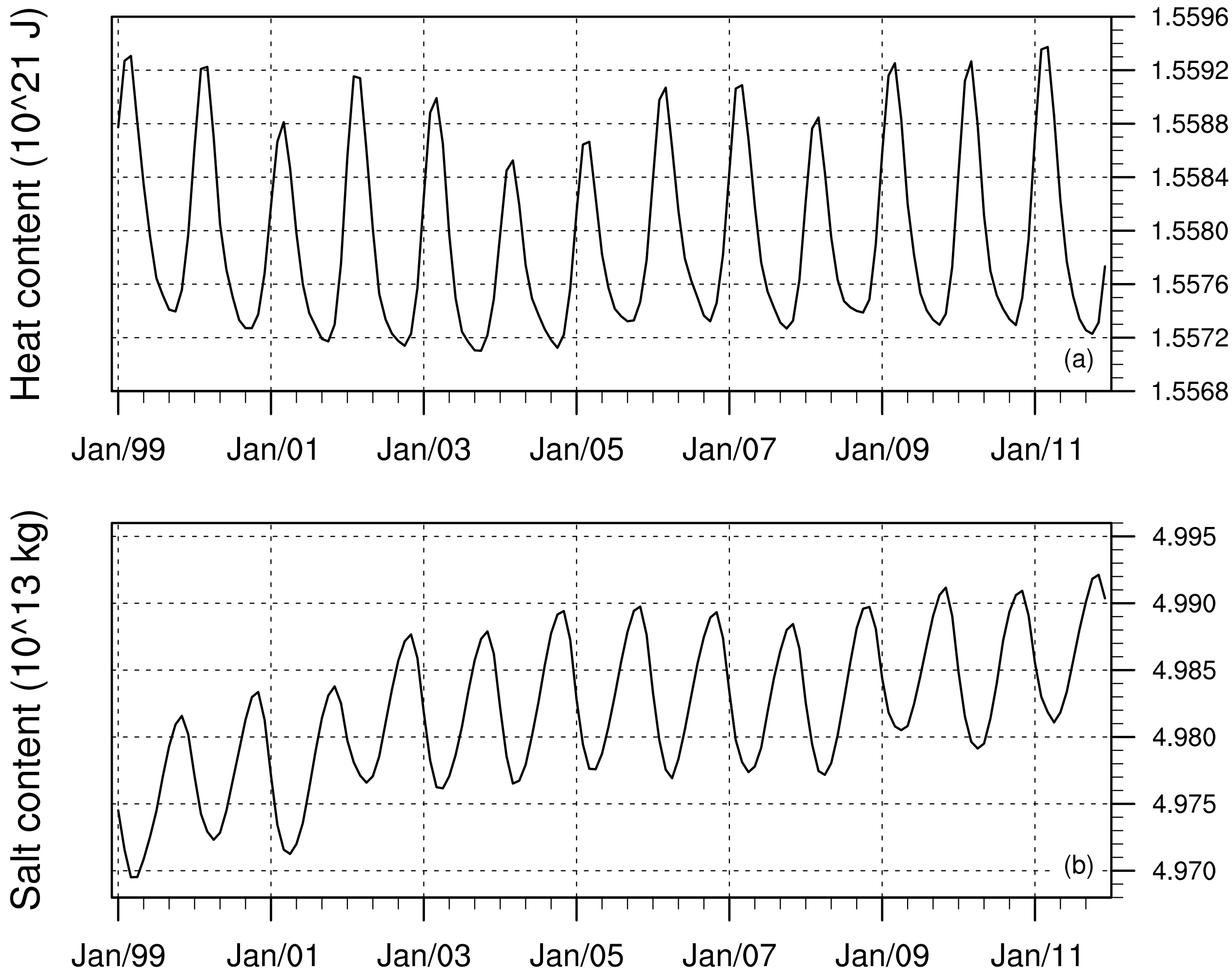

Figure 3: Time series of the total (a) heat and (b) salt content of the whole Antarctic shelf sea, calculated using Eqs. (1-2).

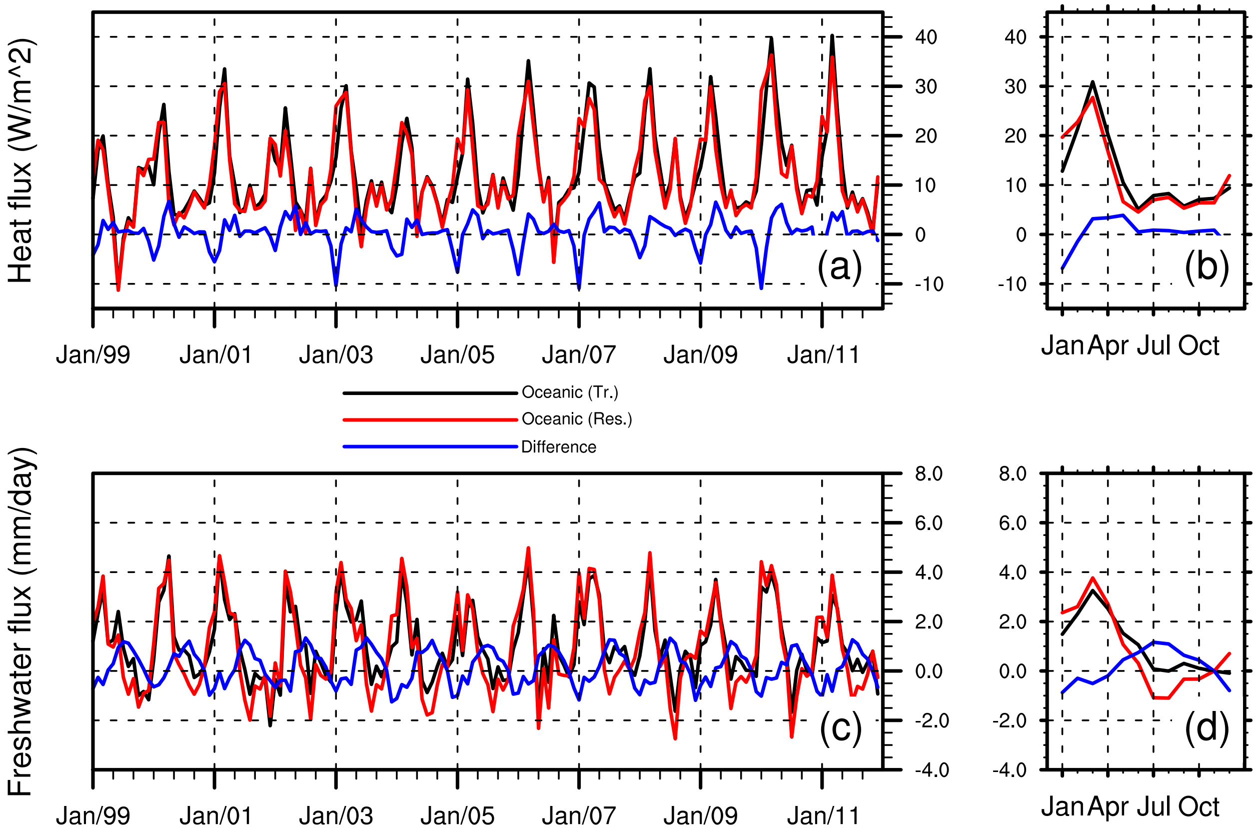

Figure 4: Time series of two different estimates of the oceanic (a) heat and (c) salt exchanges are shown. The tracer-based estimates (black curves) are obtained using two tracers C_T and C_S for heat and salt exchanges, respectively, as defined in Eqs. (5) and (8). The other estimates are computed as the residuals (red curves) of the total content change minus surface flux, where the surface flux is obtained as a model output. The differences of the two estimates are shown (blue curves). Corresponding annual cycles of the time series are shown in panels (b) and (d).

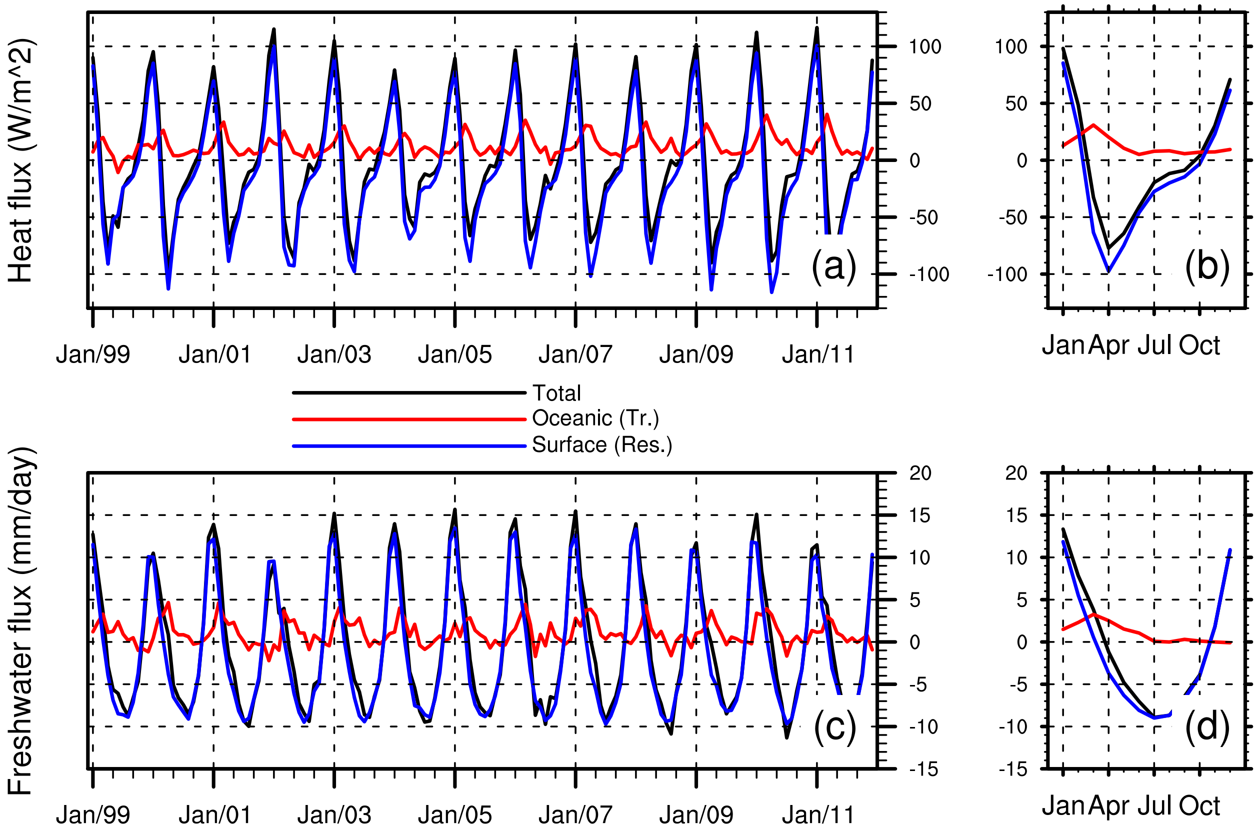

Figure 5: (a) Time series of the total heat content change of the entire Antarctic shelf sea (black curve) is shown with the cross shelf heat exchange, as well as the surface heat exchange. The oceanic heat exchange is based on the tracer method (red curve; Eq. (5)). The surface heat exchange (blue curve) is computed as a residual of the total minus the oceanic heat exchanges, Eq. (6). Annual cycles of the heat exchanges are shown in panel (b). Panels (c-d) are the same as panels (a-b), except for the freshwater flux, using Eqs. (8-9).

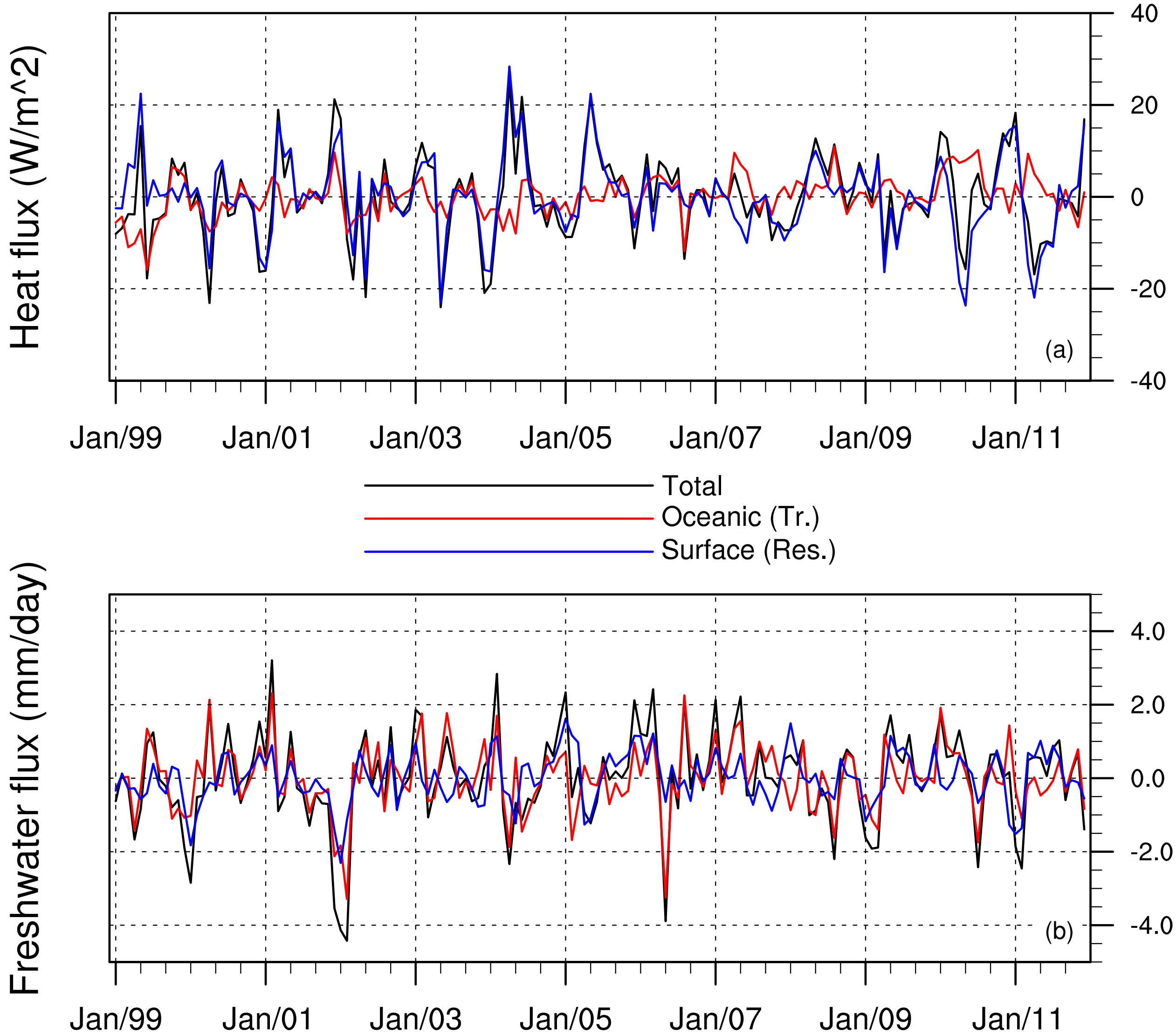

Figure 6: Time series of (a) heat and (b) freshwater fluxes as in Figs. 5a,c, except that the average seasonal cycles (Figs. 5b,d) are removed.

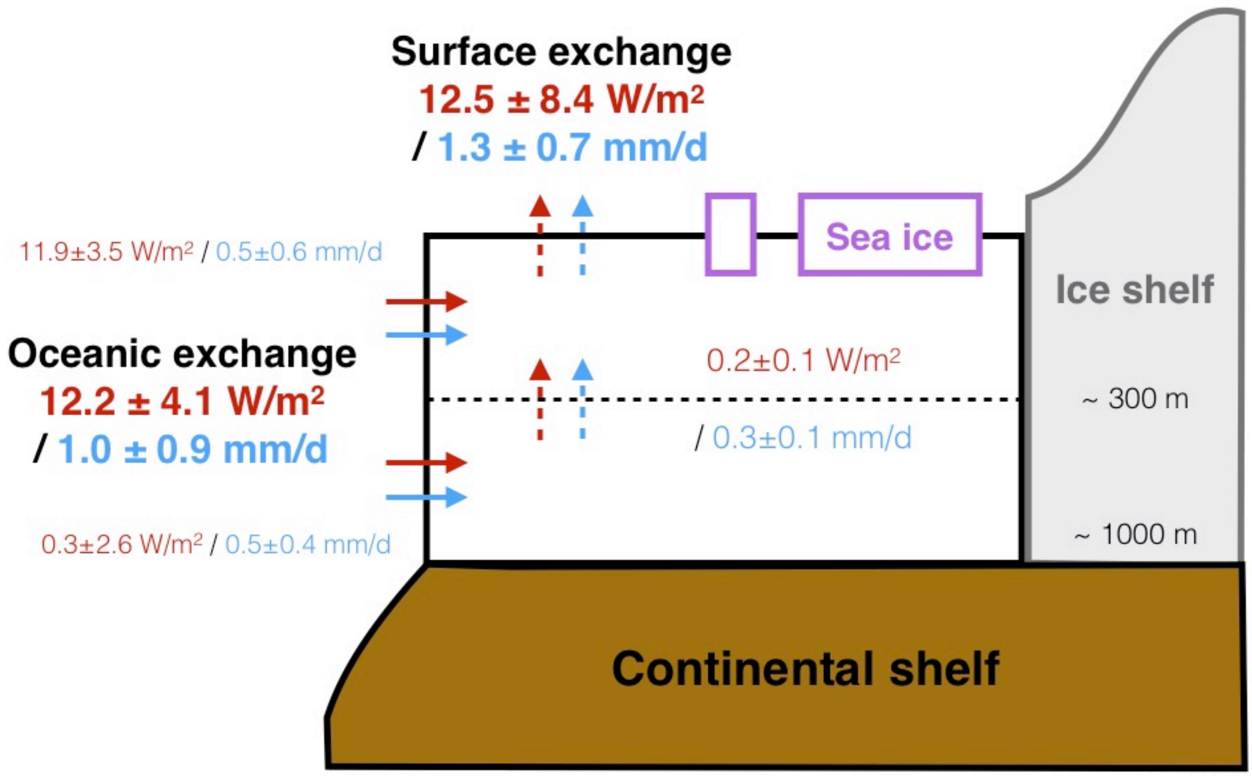

Figure 7: A schematic diagram showing the heat and freshwater budget of the whole Antarctic shelf sea. Time mean values of heat and freshwater fluxes are shown with corresponding standard deviations, which are obtained after the seasonal cycle and the linear trend are removed. There are four boundaries of the shelf sea (box in the middle) with the Southern Ocean (north), the Antarctic ice shelf (south), the Antarctic continental shelf (bottom), and the atmosphere and sea ice (top). The heat and freshwater fluxes are shown in red and blue colors, respectively. Arrows indicate direction of the flux. Because of the lack of the ice shelf in our model, the ice shelf cavity, as well as the heat and freshwater exchange with the ice shelf, are not included.

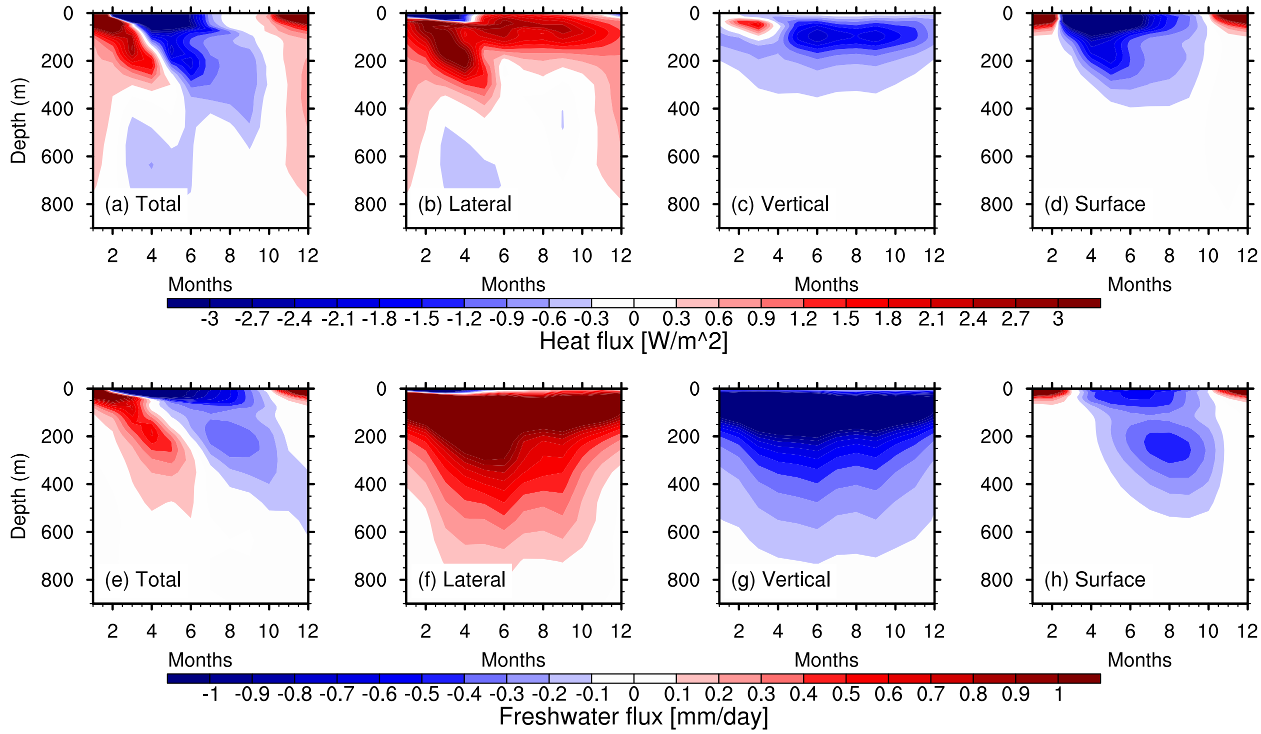

Figure 8: (a) Monthly climatology of the total heat content change with depth, which is computed by integrating Eq. (3) for each vertical layer of the model. (b) The oceanic heat exchange is divided in to two components: the lateral and vertical fluxes. The lateral flux is obtained as for panel (a), by integrating Eq. (5) for finite vertical depths, but then by subtracting the vertical exchange. (c) The vertical exchange is sum of vertical diffusion and advection of tracer C_T, saved as a model output. (d) The surface exchange is obtained as a residual of (a) minus (b + c). Panels (e-h) are the same as panels (a-d), except for the freshwater flux using Eqs. (7-8).

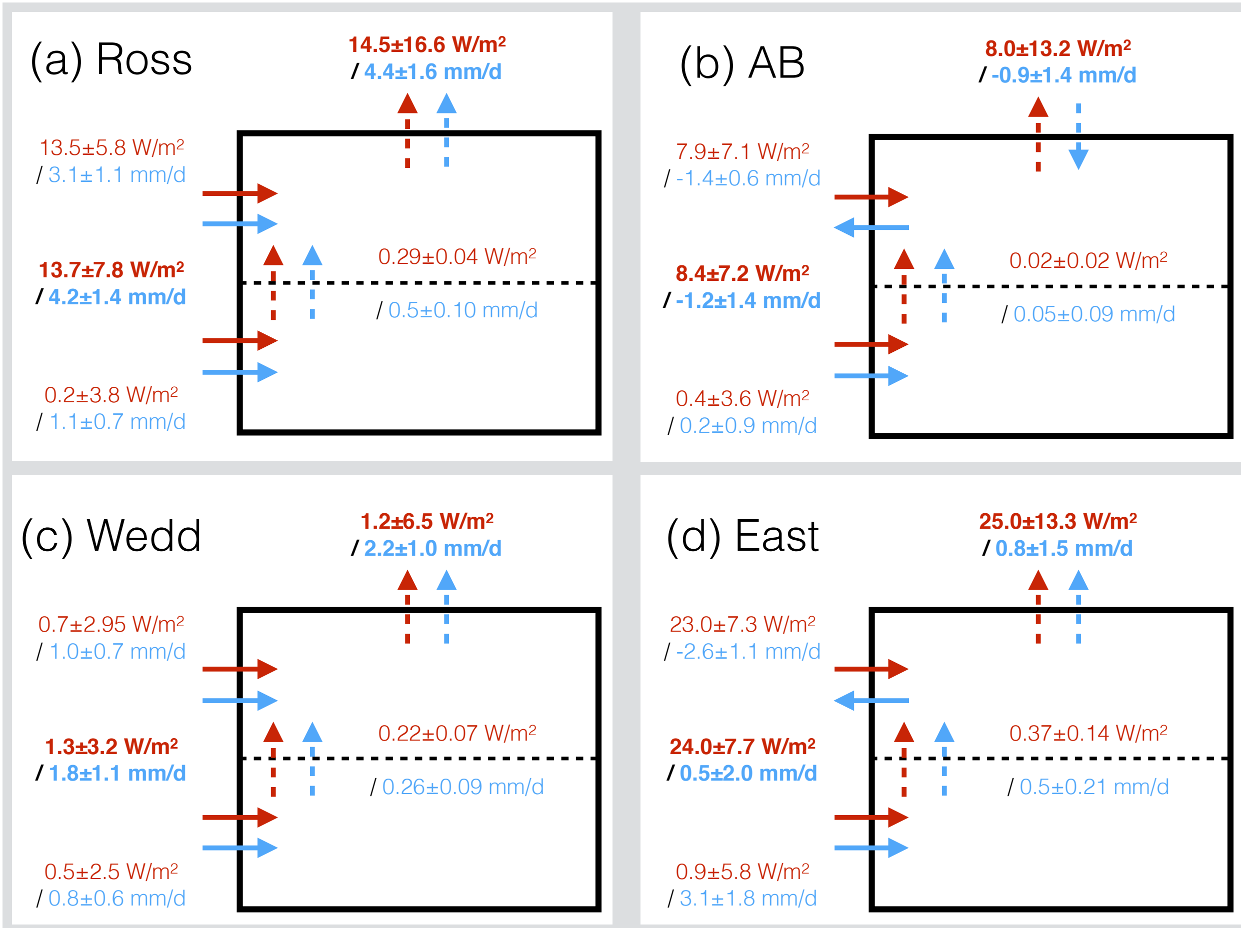

Figure 9: The same heat and freshwater budgets as in Fig. 7, except for the local shelf seas shown in Fig. 1: (a) Ross, (b) Amundsen-Bellingshausen, (c) Weddell, and (d) East Antarctic shelf seas.